Materials Advances

ROYAL SOCIETY OF CHEMISTRY

PAPER

View Article Online
View Journal | View Issue

Cite this: *Mater. Adv.*, 2025, 6, 2600

Electrochemical aptasensing platform based on nanolaminated MAB/MBene phases for the efficient detection of 11-deoxycortisol†

Amina Rhouati,‡[a] Rawan Ramadan Mohamed,‡[a] Madhurya Chandel,[b] Karamullah Eisawi,[c] Michael Naguib,[c] Agnieszka Jastrzębska[b] and Mohammed Zourob*[a]

Nanolaminated materials have attracted much attention because of their advantageous physicochemical properties. MXene-type materials have shown great promise in the field of biosensors. However, MBenes have not been extensively explored in this field. Therefore, herein, we compared the properties of nanolaminated MAB phases and ML (Multilayer) MBene, and these phases were used in the development of an electrochemical aptasensing platform. The microarray platform comprised two working carbon electrodes, which were modified with gold nanoparticles (AuNPs) and multi-walled carbon nanotubes (MWCNTs). The efficiency of ML MBene was compared with its parental MAB phase by modifying the electrodes. Owing to its better electrochemical results, MBene was further selected for application in an aptasensor. MBene/AuNPs/MWCNT-modified electrode was functionalized with an aptamer specific to the hormone 11-deoxycortisol (11-DCL). The resulting aptasensor showed an outstanding limit of detection of 0.014 pg mL^{-1} for 11-DCL, in relation to the determination range of 0.01 to 100 pg mL^{-1}. In addition, the aptasensor showed excellent selectivity towards interfering agents and good applicability by validating the results of real serum samples.

Received 29th November 2024,
Accepted 21st February 2025

DOI: 10.1039/d4ma01181c

rsc.li/materials-advances

Introduction

Recently, nanolaminated materials have gained much attention in different research fields because of their outstanding physicochemical properties.[1] They are mainly composed of transition metal carbide, nitride, or boride layers. We distinguish MAX phases with the general formula of $M_{n+1}AX_n$ and MAB phases with the chemical formulae of MAlB, M_2AlB_2, M_3AlB_4, and M_4AlB_6, where M is an early transition metal, A is a 13th or 14th group element (such as Al or Si), n = 1–4, X is carbon and/or nitrogen, and B is boron.[2,3] MAX phases consist of hexagonal crystal structures with a single $P63/mmc$ symmetry, where the A atoms separate the M and X layers.[4] However, MABs possess an advanced structure with variable symmetries, including orthorhombic (*Cmmm*, *Pmmm*, *Cmcm*, and *Immm*), tetragonal, and hexagonal ($P\bar{6}m_2$) lattices.[5] MXene is synthesized by removing the aluminum layer from the MAX precursor, resulting in the $M_{n+1}X_nT_x$ structure, where X refers to carbon and/or nitrogen and T_x refers to the terminal functional groups.[6] As in the case for MAX phases and MXene, the etching and delamination of MABs will result in 'MBene' structures, which are also called transition metal boridenes.[7] Apart from different stoichiometries, MAB–MBene presents various modes of 2D layer sandwiching and structural transformations other than those exhibited by MAX–MXene systems.[7,8] MBenes are especially interesting in various biotechnological applications. They can be used as anti-cancer agents[9] and can exhibit antibacterial and anti-inflammatory properties owing to the presence of boron in their structure.[10]

MAB phases are stable transition metal borides composed of M and A atoms stacked in an orthorhombic lattice. B-coordinated M atoms are bonded in trigonal prisms and are perpendicular to the A layers. Short distances separate the boron atoms, forming a zigzag shape. After Al removal, the etching product 'MBene' is generated; it is composed of a multi-layered structure with open slit-shaped pores.[5,7] Both MBene and MAB phases have unique properties that result from the thermal, chemical, and mechanical stability of the binary borides as well as the alternating layers of the

[a] Department of Chemistry, Alfaisal University, Al Zahrawi Street, Al Maather, Al Takhassusi Road, Riyadh 11533, Saudi Arabia. E-mail: mzourob@alfaisal.edu
[b] Warsaw University of Technology, Faculty of Mechatronics, św. Andrzeja Boboli 8, 02-525 Warsaw, Poland
[c] Department of Physics and Engineering Physics, Tulane University, New Orleans, LA 70118, USA

† Electronic supplementary information (ESI) available. See DOI: https://doi.org/10.1039/d4ma01181c

‡ Equal contribution.

intermetallic and boride subunits.[8] They have also been reported as excellent electrochemical catalysts owing to their unique structures and inherent electronic properties.[11] Farhanah *et al.* studied the electrochemical properties of different MAX and MAB phases. To demonstrate their potential application in electrochemical sensors, the authors determined the heterogeneous electron transfer (HET) rate for each material. The experimental results showed that MABs exhibited a higher HET rate than MAX, where MoAlB has the highest rate with a k^0_{obs} of 1.65×10^{-3}.[3] Moreover, it has been reported that MBenes exhibit exceptional electronic conductivity and stability.[12] Despite that, the application of MAB phases in electrochemical aptasensors has not been reported yet.

Our study aims to explore the applicability of multilayer (ML) MBene and its parental MoAlB phase in the electrochemical biosensing of 11-deoxycortisol (11-DCL), a corticosteroid hormone which contributes significantly as a direct precursor for cortisol.[13] The steroidogenesis pathway involves a series of enzymes, converting cholesterol into pregnenolone, which is then converted into 17-OH pregnenolone, 17-OH progesterone, 11-deoxycortisol, and finally cortisol.[14] Deficiencies in the different enzymes ensuring the steroidogenic pathway, including 11-β hydroxylase, result in adrenal diseases such as congenital adrenal hyperplasia (CAH), which is characterized by low levels of cortisol and the accumulation of steroid precursors, including 11-DCL.[15] This variation is mainly due to the fact that hydroxylation of 11-DCL into cortisol is blocked in patients suffering from (11-β-hydroxylase deficiency) OHD.[16] 11-DCL has also been reported as a biomarker for hypercortisolism and adrenocortical carcinoma.[17] Monitoring 11-DCL levels is thus of great importance in the diagnosis of adrenal diseases and identifying deficient steroidogenic enzymes involved in cortisol biosynthesis.[18]

Conventionally, 11-DCL measurement is based on chromatographic techniques such as LC–MS/MS (liquid chromatography–mass spectroscopy/mass spectroscopy) and LC/tandem MS.[16,19,20] Immunoassays have been also reported for 11-deoxycortisol determination in plasma *via* commercial antibodies.[21,22] Despite the simplicity of immunoassays, antibodies are expensive, lack stability and specificity, and suffer from batch-to-batch variations.[23] In this context, aptamers have appeared as new biorecognition molecules that mimic the antibodies' activity. They are ssDNA or RNA generated by systematic evolution of ligands by exponential enrichment (SELEX). Their simple and low-cost chemical synthesis makes them more stable and affordable bioreceptors for screening methods.[24] Different aptamers have been selected and applied for steroid hormone determination, including progesterone, testosterone and cortisol.[25–27] In 2019, we reported on the first aptamer for 11-deoxycortisol, showing a high affinity with a dissociation constant of 0.65 nM. Subsequently, we used this aptamer in the voltammetric detection of 11-deoxycortisol, giving excellent characteristics.[28] To the best of our knowledge, this aptamer has not been integrated in another aptasensing platform. Herein, we combine the excellent binding ability of the 11-DCL aptamer with the outstanding electrochemical characteristics of the MoAlB MAB phase, and after Al etching the ML MBene, to construct a label-free aptasensor.

To demonstrate the applicability of the ML MBene and MAB nanolaminated materials in electrochemical sensing, we fabricated a dual biosensor, where we modified the two different electrodes with the MAB phase (MoAlB) and ML MBene, separately. Cyclic voltammetry (CV) and electrochemical impedance spectroscopy were employed to compare the electrochemical properties of the MAB phase and ML MBene. Then, the modified electrodes were functionalized with an 11-DCL aptamer, and the analytical performance of the two resulting aptasensors was investigated. Better results were obtained with the MBene-based aptasensor. The applicability of the developed aptasensor in serum samples was also demonstrated, as well as its cross-reactivity against other hormones.

Experimental

Materials and reagents

Hydrochloric acid (HCl) with 37% (v/v) concentration from Merck; sodium hydroxide (NaOH, 0.1 M), 30% (v/v) water solution of hydrogen peroxide (H_2O_2) from Chempur, and double-distilled water were used. Molybdenum boride (MoB, 325 mesh, 99%, Alfa Aesar) and aluminum (Al, 325 mesh, 99.5%, Thermo Scientific Chemicals) were used for MoAlB synthesis. All chemicals were used without further purification.

The ssDNA aptamer (DC 17), specific to 11-deoxycortisol and conjugated to a thiol group, was synthesized and purchased from Metabion Company, Germany. The sequence was as follows: 5′-Thiol-TAA CAG ACG TCT CCC AAG CCA TGA AAA TTA GCC CAA CTC ATA GGA CCA TAA CGC CCT ACC-3′. The aptamer was previously selected by our group, and it showed a high affinity for 11-deoxycortisol with the low dissociation constant of 0.65 nM. This aptamer also showed a high selectivity towards steroid hormones cortisol, corticosterone, and pregnenolone.[28] 11-Deoxycortisol, 17-pregnolenone, progesterone and estradiol were purchased from Cerilliant (Texas, United States). The aptamer and the different hormones were diluted in binding buffer (50 mM Tris, pH 7.5, 150 mM NaCl and 2 mM $MgCl_2$), pH 7.4. Potassium ferrocyanide [$K_4Fe(CN)_6$], potassium ferricyanide [$K_3Fe(CN)_6$], PBS, tris, sodium chloride, magnesium chloride, bovine serum albumin (BSA) and human serum were purchased from Sigma-Aldrich, Germany.

Synthesis of the MoAlB MAB phase

The MoAlB MAB phase was synthesized by mixing MoB and Al with a molar ratio of 1 : 1.2. Yttria-stabilized zirconia (YSZ) balls were added to the mixture, which was then loaded into a Turbula T2F mixer for 3 h at 56 rpm. After mixing, the powder mixture was cold-pressed into a 1-in. diameter pellet and placed in an alumina crucible at the center of an alumina tube furnace. The crucible was heated initially to 750 °C for 2 h, followed by heating to 1550 °C for another 2 h, with a heating rate of 10 °C min^{-1} under an argon (Ar) atmosphere at a flow rate of 100 standard cm^3 min^{-1} (SCCM). Once the heating

process was complete, the furnace was allowed to cool naturally to room temperature. The resulting MoAlB pellet was crushed and ground using a mortar and pestle, then sieved through a 325-mesh sieve using a Gilson 3 in Vibratory Sieve Shaker to achieve a particle size below 45 μm for further processing.

Etching of Al from the MAB phase (MoAlB)

Initially, 100 mg of MoAlB was stirred in 0.1 M HCl for 2 h, then washed with distilled water until a pH value of 6 was obtained. After that, the washed precipitate was slowly transferred into 20 mL of 0.6 M HCl with constant stirring, followed by sonication for 2 min. After that, 100 μL of H_2O_2 (30%) solution was added dropwise, and the lid of the Teflon container was closed. Then, the Teflon container with the reaction mixture was fitted into the microwave reactor. The reaction started at 150 °C with 480 W power for 120 minutes. After the reaction, the supernatant was yellow and the precipitate was black. The mixture was washed five times *via* centrifugation. The pH of the mixture became 6. The black precipitates were then collected for further study.

Materials characterization

The morphology was studied using scanning electron microscopy (SEM) and energy-dispersive X-ray (EDS) spectroscopy (Hitachi SU3500 and Hitachi S5500, Hitachi, Tokyo, Japan). The samples for SEM imaging and EDS spectra were prepared on a carbon-coated copper grid. X-ray diffraction (XRD) patterns were measured to determine the purity and crystal structure of the samples using a Bruker D8 Advanced system (Billerica, MA, USA).

Electrochemical analysis

All electrochemical measurements, including cyclic voltammetry, electrochemical impedance spectroscopy and square wave voltammetry (SWV), were conducted using a Metrohm (Switzerland) Autolab potentiostat, PGSTAT302N model. The potentiostat was connected to a personnel computer and operated by the Nova 1.11 software. The aptasensor was fabricated on dual screen-printed carbon electrodes modified with multi-walled carbon nanotubes and gold nanoparticles (SPCE/MWCNTs/AuNPs) (Aux: carbon; Ref: Ag) (Metrohm DropSens, Inc. Asturias, Spain).

Morphologic studies of the SPCE surface were performed at each step *via* scanning electron microscopy in an SEM JEOL Ninja microscope with a discharge voltage of 20 kV. All samples were sputter-coated with 2 nm platinum before characterization. The electron field was 5 kV.

Fabrication of the electrochemical aptasensor and 11-DCL detection

A microarray composed of two working electrodes modified with MWCNTs and AuNPs was used to construct the electrochemical aptasensor. The first electrode was modified with the MAB phase, and the second was modified with its derivative ML MBene. MoAlB and ML MBene solutions were prepared by dissolving the powder (1 mg mL^{-1}) in distilled water under sonication for 10 minutes. Then, 10 μL of each solution were drop cast on the first and the second MWCNTs/AuNP-modified carbon electrodes, respectively. The surface was then left to dry at room temperature, and rinsed with PBS to remove the excess MoAlB and ML MBene materials. Afterward, 10 μL of the thiolated DNA aptamer specific to 11-DCL was added to both electrodes of the microarray. The ssDNA aptamer was allowed to interact with the modified surface at 4 °C overnight in a water-saturated environment. To block the remaining active sites, the MAB/MBene/MWCNT-AuNP-SPCEs were incubated with a solution of 1% BSA (bovine albumin serum) for 40 minutes at room temperature. Finally, the surface was washed with PBS and stored at 4 °C for further use. Each step of the fabrication process was characterized by CV at a scan rate of 100 mV s^{-1} within a potential range of −1 to 1 V for MoAlB and ML MBene in 5 mM ferro/ferricyanide redox solution prepared in PBS buffer at a pH of 7.4.

For detection experiments, 10 μL of the 11-DCL solution prepared in binding buffer was dropped onto the SPCE-MWCNT-AuNP-MAB phase/MBene-11-DCL aptamer and incubated for 20 minutes at room temperature. Increasing amounts of 11-DCL, ranging from 0 to 100 pg mL^{-1} and prepared in BB, were tested. After PBS washing, the electrode surface was immersed in 5 mM of $[K_4Fe(CN)_6]/[K_3Fe(CN)_6]$ for electrochemical measurements. The square wave measurements were recorded in the range of −0.3 to 0.5 V at an interval time of 0.04 s, frequency of 25 Hz, a scan rate of 125 mV s^{-1}, amplitude of 20 mV, and step potential of −5 mV.

Selectivity and real sample applications

Cross-reactivity studies were carried out to confirm the specificity of our aptasensor for 11-DCL determination. For selectivity, the aptamer-functionalized electrode was tested with three potential hormones: 17-pregnolenone, progesterone, and estradiol. Then, the analytical response of the biosensor towards the specific analyte was compared with that obtained with the interfering hormones. In parallel, testing the aptasensor performance in real serum samples was also performed. Serum samples were first diluted by 1 : 100 in binding buffer, then spiked with different amounts of 11-DLC (0.01, 0.05, and 0.1 pg mL^{-1}). For both selectivity and serum sample applications, we followed the same aptasensing protocol described above.

Results and discussion

Various reports have highlighted the excellent electrochemical properties of the MAB phase and MBene. They are characterized by high electronic conductivity and good stability.[3] They have also been reported to be excellent catalysts.[11] Therefore, we combine the advantages of aptamers as biorecognition elements with the electrochemical properties of MAB/MBene to develop an electrochemical aptasensing platform to detect 11-deoxycortisol. Fig. 1 depicts the etching of Al from the MAB phase (MoAlB) to ML MBene, the fabrication of the MoA1B and

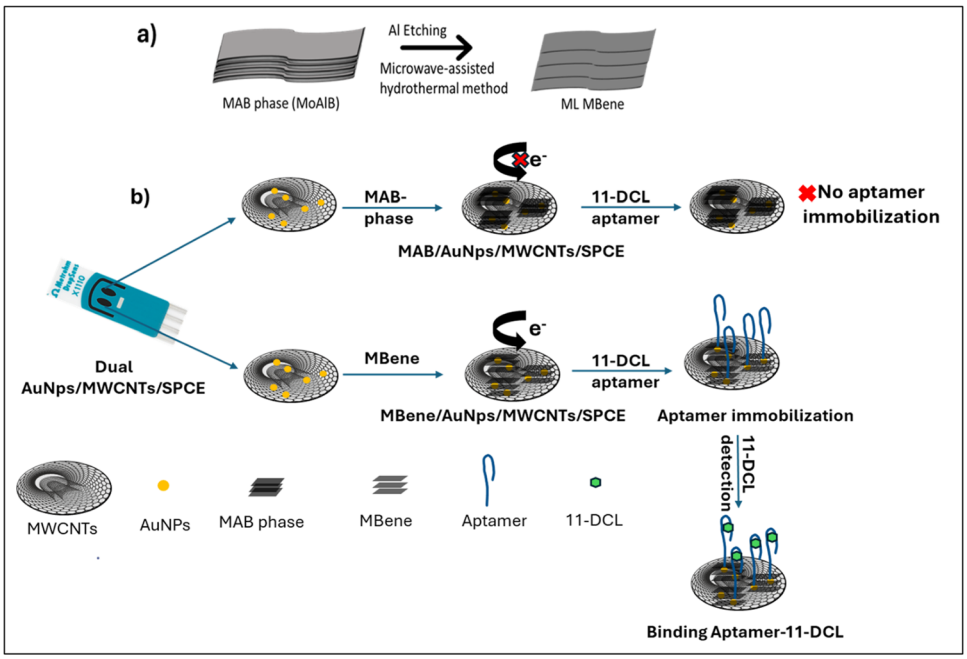

Fig. 1 Graphical representation of Al etching from the parent MAB phase (MoAlB) using microwave-assisted hydrothermal method (a) and fabrication steps of the MAB-phase and MBene-modified AuNPs/MWCNTs/SCPE for 11-DCL detection (b).

MBene modified electrodes and the principle of 11-DCL aptasensing.

Structural analysis

Here, the microwave-assisted hydrothermal method was employed based on the etching solution of 0.6 M HCl and H_2O_2 (from 30% water solution). Then, we performed energy-dispersive spectroscopy (EDS) measurements and scanning electron microscopy (SEM) to analyze the outcome of our Al etching. SEM images reveal the initial MAB phase (MoAlB) in its unetched, densely packed state, as depicted in Fig. 2(a). In Fig. 2(b), the ML (multilayer) MBene was deeply etched and formed an accordion-like structure, similar to Mxene after etching from the MAX phase.[29,30] SEM images confirm better etching, and the cavities range from nanometer to micrometer scale. Fig. 2(c) and (d) show the EDS spectra of MoAlB and ML MBene, respectively, revealing that over 60% of Al was etched from MoAlB using the mentioned technique. Elemental mapping for MoAlB (Fig. S1, ESI†) and ML MBene (Fig. S2, ESI†) also demonstrate the formation of a multilayer-like accordion structure with reduced Al content. Tables S1 and S2 (ESI†) provide each element's weight and atomic percentages, confirming the Al percentage reduction (from 20 wt% to 9 wt%) after etching from MoAlB.

We further recorded the X-ray diffraction (XRD, Fig. 2(c)) patterns to understand the structure better. The XRD pattern of the MAB phase MoAlB matches well with previous reports (and PDF card no. 01-072-1277), while changes are visible after the etching.[31,32] If complete etching of Al were achieved, the (0k0) reflections would broaden and shift to lower angles, while other reflections (such as (110), (022) and (204)) would weaken significantly or disappear completely. Here, most minor-intensity peaks (such as (110), (021), (022) and (204)) of MoAlB nearly disappear in the case of ML MBene. This indicates that the Al content has decreased compared to MoAlB. At the same time, the intensity of the (0k0) peaks (such as (020), (040), (060)) increases by 2 times in ML MBene. The increasing intensity indicates a higher degree of order, arrangement, and crystalline phase in ML MBene. Further, the MoAlB MAB phase and Al etched ML MBene were used to fabricate the electrode to understand their electrochemical behaviour for aptasensing.

SEM characterization was also carried out to study the surface morphology of the working electrode, before and after addition of the MAB phase and ML MBene. The SEM images are shown in Fig. 3(a) for the SPCE modified with MWCNTs and AuNPs, Fig. 3(b) for the electrode surface after the addition of the MAB phase, and Fig. 3(c) for the SPCE modified with MWCNTs, AuNPs, and ML MBene. Fig. 3(a) shows the tubular structures distributed on the surface corresponding to the carbon nanotubes, while we observed bright spots that refer to the gold nanoparticles. By comparing the SEM images shown in Fig. 3(b) and (c), we note that the MAB phase-modified electrode does not exhibit spaced layers. On the other hand, the surface morphology of the electrode modified with MBene shows well-defined intercalated multilayers Fig. 2(c). This laminated structure enlarges the surface area, thus improving the rate of aptamer immobilization.[33] The SEM images align well with our previous study, where we demonstrated the successful aluminum etching from the MAB phase into the laminated MBene structure.[34]

Electrochemical characterization

Cyclic voltammetry and electrochemical impedance were applied to the MWCNTs/AuNPs/SPCE surface before and after

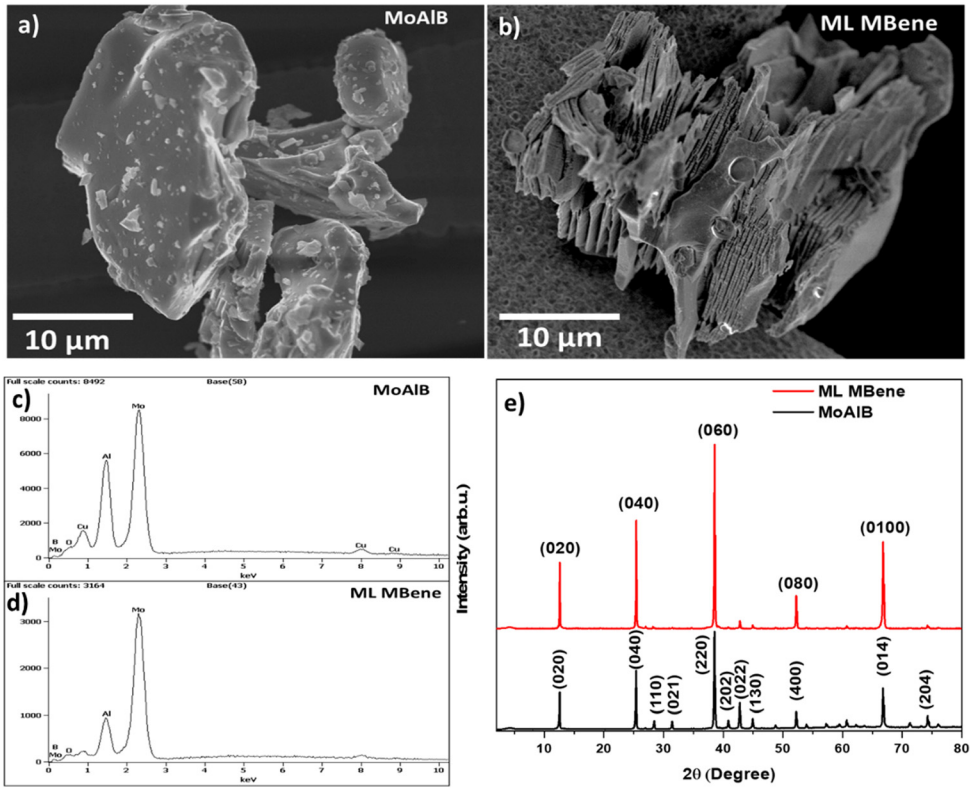

Fig. 2 SEM images of (a) MAB phase MoAlB and (b) ML (multilayer) MBene after Al etching. EDS spectra of (c) MoAlB and (d) ML MBene. (e) XRD diffraction patterns of MoAlB and ML MBene.

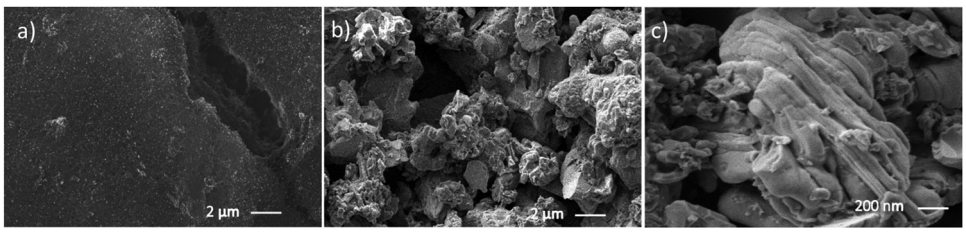

Fig. 3 SEM images of (a) AuNPs/MWCNTs/SPCE, (b) MAB phase-modified AuNPs/MWCNTs/SPCE and (c) ML MBene-modified AuNPs/MWCNTs/SPCE. Transmission electron microscopy studies performed in our previous work have shown the presence of interlayered cavities in the MBene structure and an orthorhombic lattice in the corresponding diffraction pattern.[5]

each modification step to study the electrochemical properties of the MoAlB MAB phase and ML MBene. CV was performed in a ferro/ferrocyanide redox solution (5 mM) at a scan rate of 100 mV s^{-1} within a potential range of −1 to 1 V. EIS was carried out using the same electrolyte over the frequency range from 10^5 to 1 Hz, a potential of +0.4 V and an amplitude of 10 mV. Fig. 4(a) and (b) show the cyclic voltammograms obtained for the MAB phase and ML MBene, respectively, while Fig. 4(c) and (d) display the corresponding impedance spectra. We noted that the voltammograms represented by the black curve corresponding to the screen-printed electrode modified with gold nanoparticles and multi-walled carbon nanotubes exhibit well-defined oxidation and reduction peaks. This behavior is due to the high conductivity of AuNPs and their high surface-to-volume ratio.[35] On the other hand, MWCNTs offer high electron transfer ability and high strength, owing to their high length-to-diameter ratio of up to 132 000 000 : 1.[36] Following that, the two working electrodes were modified with the MAB phase and ML MBene separately. We note that the voltammogram represented by a red line in Fig. 4(b) (parental phase) exhibits an oxidation peak that is much lower than that of ML MBene in Fig. 4(a). An oxidation current of around 250 µA was obtained for ML MBene in comparison to the oxidation current of 100 µA for the MAB phase. This difference could be explained by the fact that ML MBene has well-pronounced layers as compared to its parental phase, which is characterized by a closely packed laminar structure. Like the MAX phases, MoAlB MAB phase etching by Al removal also

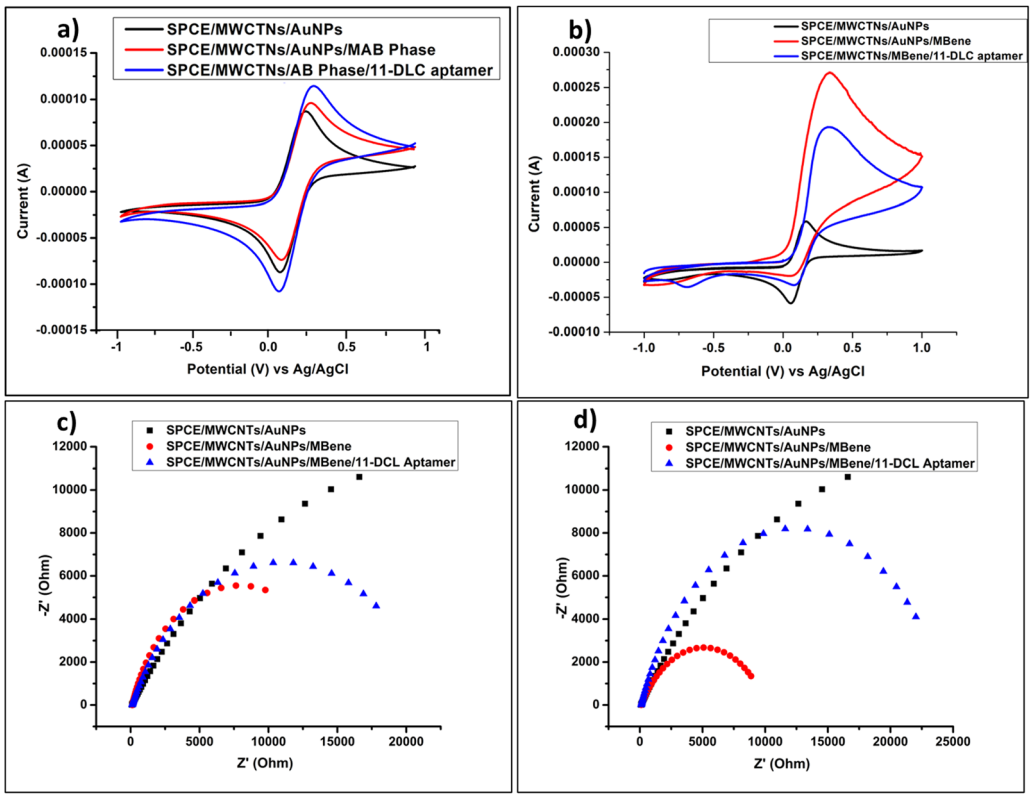

Fig. 4 Surface characterization of the fabrication steps of the aptasensor: CV analysis on (a) the MAB phase/MWCNTs/AuNP-modified SPCE and (b) MBene/MWCNTs/AuNP-modified SPCE. Cyclic voltammograms were recorded in 5 mM ferro/ferricyanide redox solution prepared in PBS buffer at a pH of 7.4 at a scan rate of 100 mV s^{-1}, Nyquist plots for the impedance measurements corresponding to the MAB phase/MWCNTs/AuNP-modified SPCE (c) and MBene/MWCNTs/AuNPs modified SPCE (d). EIS spectra recorded in the same electrolyte over the frequency range from 10^5 to 1 Hz at a potential of +0.4 V and an amplitude of 10 mV. Information on the used circuit and the fitting values are provided in the (ESI†).

creates an empty space between Mo and B layers. The resulting pores or cavities promote electron transfer to the sensing surface, which explains the significant increase in the oxidation peak current (I_{pa}).[37] This behavior could also be attributed to the surface reactivity resulting from the surface terminations of ML MBene. These findings are supported by the red EIS spectra in Fig. 4(c) and (d), where the resistance decrease was more significant in the MBene-modified electrode. In the last step, we immobilized our biomolecular receptor (aptamer) on both MAB phase and Ml MBene-modified SPCEs. The corresponding cyclic voltammograms and EIS spectra (blue curve) are shown in Fig. 4(a)–(d), respectively. When analyzing the oxidation current peaks, we observe a significant decrease in the case of the ML MBene/MWCNTs/AuNPs/SPCE. In contrast, the MAB phase/MWCNTs/AuNP-modified SPCE shows a slight increase after adding the aptamer. In parallel, impedance results show a remarkable increase in the surface resistance for the ML MBene-modified surface and a slight decrease in MAB-phase/SPCE. These findings confirm the successful immobilization of the aptamer occurring on the ML MBene-modified surface, as opposed to the electrodes modified with its parental MAB phase. This can be explained by the presence of cavities in the ML MBene structure.[5] We hypothesize that these holes enable the covalent interaction between the AuNPs on the SPCE surface and the thiol group conjugated to the aptamer sequence. Conversely, the access of the thiolated DNA to the gold nanoparticles was inhibited because of the packed layers of the MAB phase.

Electrocatalytic properties of the MAB phase and ML MBene-modified surfaces

Cyclic voltammetry was performed at different scan rates to investigate the kinetics of the two modified working electrodes forming the dual microarray. For that, we studied the effect of the scan rate on the redox process in 5 mM of $[K_4Fe(CN)_6]$/$[K_3Fe(CN)_6]$. Fig. 5(a) and (b) show the cyclic voltammograms recorded for the MAB phase and ML MBene, respectively, at scan rates ranging from 10 to 300 mV and a potential window of −1 to 1 V. We observe that the redox peak currents increase by increasing the scan rate, while the potential remained almost constant. Based on these findings, we plotted a linear fit of the oxidation peak (I_{pa}) and reduction (I_{pc}) peak currents as a function of the square root of the scan rate ($\nu^{1/2}$). A good linear relationship was obtained between the square root of the potential scan rate and the current with R^2 of 0.99 for both ML MBene and its parental MoAlB MAB phase. The linear equations were determined as follows: $I_{pa} = 0.187 + 9.08\nu^{1/2}$ and $I_{pc} = 0.15 - 0.1\nu^{1/2}$ for the MAB phase/MWCNTs/AuNP-modified SPCE. In parallel, the equations corresponding to the

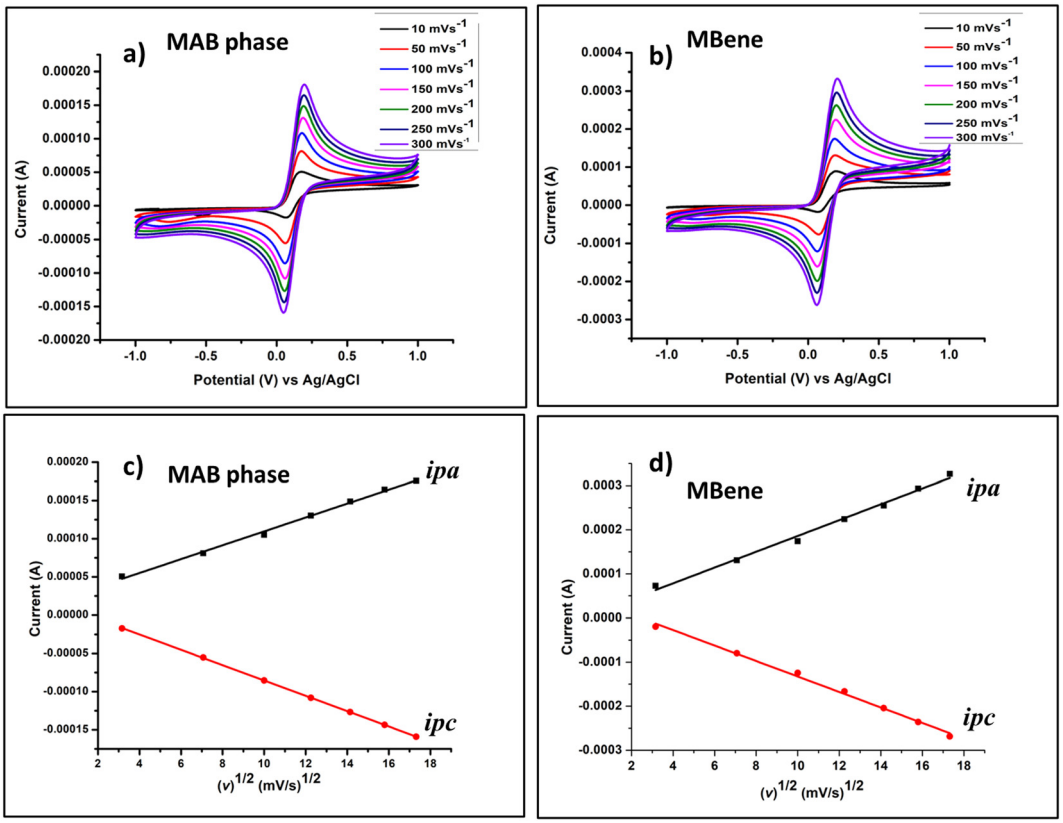

Fig. 5 Cyclic voltammograms of the (a) MAB phase/MWCNTs/AuNPs/SPCE and (b) MBene/MWCNTs/AuNPs/SPCE in 5 mM ferro/ferricyanide redox solution prepared in PBS buffer at a pH of 7.4 at different scan rates of 10, 50, 100, 150, 200, 250 and 300 mV s^{-1} and a potential window of −1 to 1 V. Plot of the anodic and cathodic peak currents *vs.* the square root of the scan rates for the (c) MAB phase/MWCNTs/AuNPs/SPCE and (d) MBene/MWCNTs/AuNPs/SPCE.

ML MBene/MWCNTs/AuNP-modified SPCE were as follows: $I_{pa} = 0.89 + 81.5v^{1/2}$ and $I_{pc} = -0.31 - 82.9v^{1/2}$. Based on these outcomes, we suggest a diffusion-controlled process for the modified surface.

Based on the linear curves shown in Fig. 5(c) and (d), the active surface area of the two MAB-phase and ML MBene-modified electrodes was estimated by using the Randles–Sevcik equation:

$$i_{pa} = 2.69 \times 10^5 \times n^{3/2} \times A \times C^0 \times D^{1/2} \times v^{1/2}$$

In the equation above, i_{pa} is the peak current, n is the number of electrons, A is the active surface area, C^0 is the concentration of the analyte, D is the diffusion coefficient of the oxidized analyte, and v is the scan rate. The electroactive surface area (A) of the two prepared electrodes was estimated according to the equation. In this study, the concentration of the $[Fe(CN)_6^{3-}]$ solution $C^0 = 5.0 \times 10^{-6}$ mol cm^{-3} was used with the number of electrons $n = 1$, and the diffusion coefficient of the electrolyte is $D = 7.6 \times 10^{-6}$. A surface area of 0.09 cm^2 was calculated for the MAB phase in comparison to the surface area (0.14 cm^2) for ML MBene. This large electroactive surface area confirms that ML MBene enhances the electron transfer through the interface sensing surface-solution.

11-Deoxycortisol determination

Given the characterization results showing that ML MBene provides a better transducing surface than the MAB phase, we designed an aptasensing platform based on ML MBene/MWCNts/AuNPs/SPCEs for 11-deoxycortisol. First, the incubation time allowing the binding of the aptamer and 11-DCL was optimized by testing different durations (5, 10, 15, 20, and 25 minutes). The electrochemical signal was analyzed by SWV using the parameters described above. Fig. 6(a) shows the analytical response $(i^0 - i)/i^0\%$ obtained for each incubation time, where i^0 is the peak current recorded before the addition of 11-DCL, and i is the current after incubation with a fixed concentration of the target (0.05 pg mL^{-1}) for different durations. An increasing response was observed by increasing the incubation time from 5 to 20 minutes, followed by a decrease at 25 minutes. Therefore, a duration of 20 minutes was selected for the binding between the aptasensor and 11-DCL.

To investigate the analytical performance of the developed biosensor, the aptamer-functionalized surface was exposed to increasing concentrations of the targeted hormone (0, 0.01, 0.05, 0.1, 10, 50 and 100 pg mL^{-1}). Then, the label-free detection of 11-DCL was carried out by SWV in the redox couple solution $[K_4Fe(CN)_6]/[K_3Fe(CN)_6]$ prepared in PBS pH 7.4. Fig. 6(b) shows the square wave voltammograms recorded for

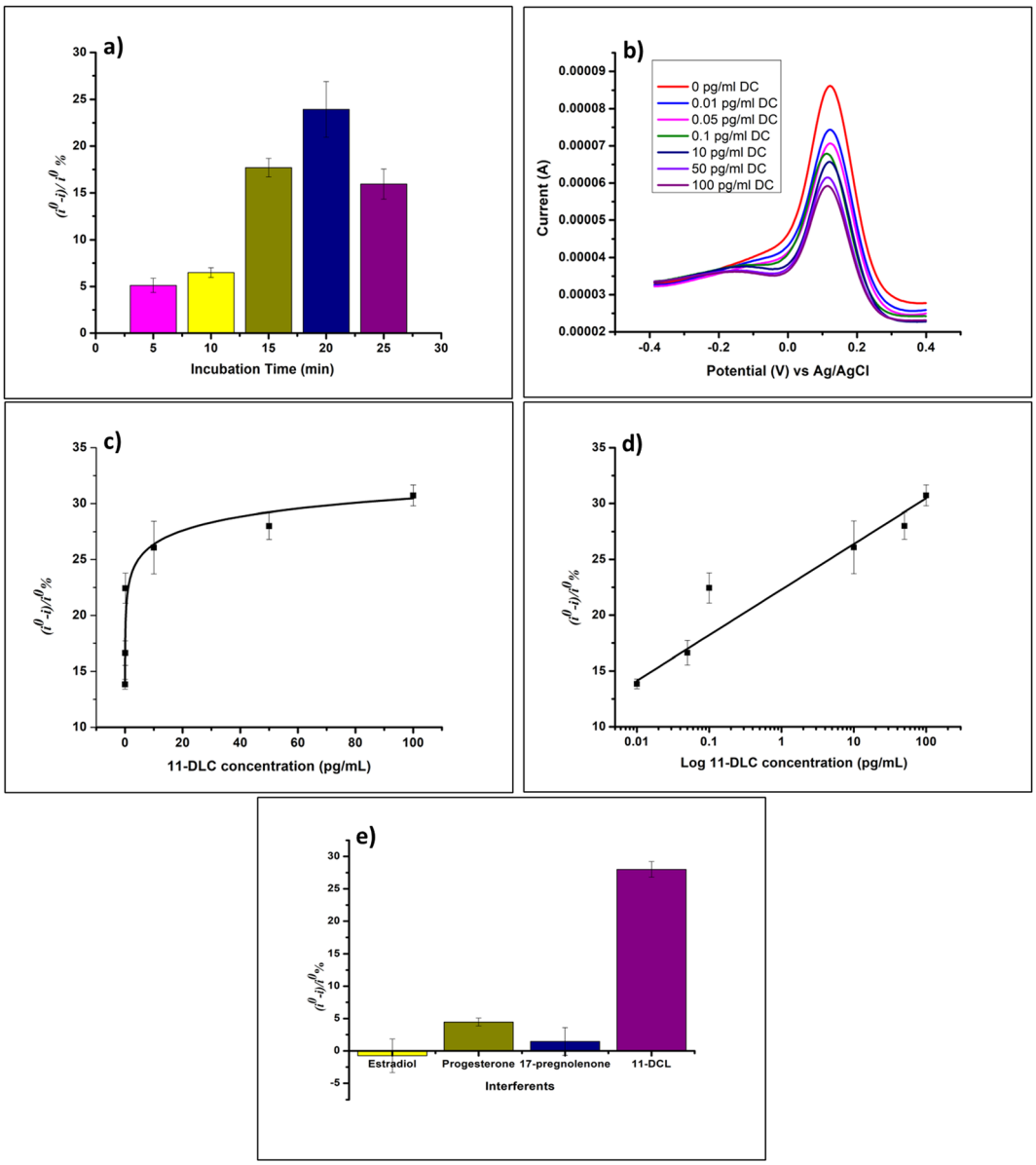

Fig. 6 (a) Optimization of the incubation time for the aptasensor-target at a fixed concentration of 11-DCL (0.05 pg mL^{-1}), (b) square wave voltammograms recorded before and after incubation of the MBene/MWCNTs/AuNPs/SPCE with increasing concentrations of 11-DCL (0, 0.01, 0.05, 0.1, 10, 50 and 100 pg mL^{-1}). The square wave measurements were recorded in 5 mM ferri/ferrocyanide in the potential range of −0.3 to 0.5 V at an interval time of 0.04 s with a frequency of 25 Hz, a scan rate of 125 mV s^{-1}, amplitude of 20 mV, and a step potential of −5 mV. (c) Plot of the aptasensor response *versus* 11-DCL concentration. (d) Plot of the sensor response ($(i^0 - i)/i^0$%) *versus* the logarithm of 11-deoxycortisol concentration (pg mL^{-1}). The error bars represent the standard deviation of three measurements. (e) Comparison of the analytical response of the MBene-based aptasensor to 10 pg mL^{-1} estradiol, progesterone, 17, pregnenolone and 11-deoxycortisol.

the tested concentrations. The results clearly show that the reduction peak currents decrease by increasing the 11-DCL concentrations. This decrease confirms the successful binding of the aptamer to its target 11-DCL, inducing the DNA conformational change to a three-dimensional structure, thus hampering the electron transfer to the transducing surface. The aptasensor response ($(i^0 - i)/i^0$%) was then calculated by using the peak current obtained without the target (i) and the peak currents obtained for each concentration of 11-DLC (i). We plotted the obtained response *versus* 11-DCL concentration in Fig. 6(c). We note that the response increased with increasing concentration, and showed a plateau between the 11-DCL concentrations of 50 and 100 pg mL^{-1}. Fig. 6(d) displays the calibration curve of the 11-deoxycortisol aptasensor; a plot of the response ($(i^0 - i)/i^0$%) against the logarithm of the target concentration in pg mL^{-1}. A good linear relationship was obtained between the aptasensor response and the logarithm of the 11-DCL concentration in the range of 0.01 to 100 pg mL^{-1}, with a R^2 of 0.97. The linear regression equation was determined as $(i^0 - i)/i^0\% = 22.29 + 4.08 \log$ 11-DCL

concentration (pg mL^{-1}). The detection limit of the aptasensor was calculated as 0.014 pg mL^{-1}, using the formula $3\sigma/b$, where σ is the standard deviation of the blank sample and b is the slope. The bar errors represent the standard error obtained from triplicate measurements for each concentration.

The obtained performance can be attributed to the synergetic effect of the used nanomaterials. The MBene layers play a critical role in enhancing the electrochemical signal, owing to their large surface and surface reactivity. In parallel, AuNPs enabled the covalent attachment of the thiolated-ssDNA aptamer. On the other hand, MWCNTs provide a highly conductive and large specific area, creating an optimum microenvironment for the MBene layers.

Specificity and real sample applicability

As mentioned in the introduction section, cortisol biosynthesis involves a series of enzymes and passes through 17-OH pregnenolone, 17-OH progesterone, and 11-deoxycortisol molecules. For that, we performed additional experiments to investigate the aptasensor specificity to 11-DCL. In brief, the ML MBene/AuNPs/MWCNTs/SPCE functionalized with 11-DCL aptamer were exposed to a fixed concentration (10 pg mL^{-1}) of some potential interfering hormones; estradiol, 17-OH progesterone and 17-OH pregnenolone. After incubation for 20 minutes at room temperature, square wave voltammetry was performed under the same conditions described above. Then, the sensor's response ($(i^0 - i)/i^0$%) was calculated for each interfering compound and compared to that obtained with the specific analyte (11-DCL). Based on the comparison shown in Fig. 6(e), we note that the response obtained for estradiol was in the negative range, while ($(i^0 - i)/i^0$%) was less than 5% for 17-OH pregnenolone. In parallel, we obtained a low response for 17-OH progesterone, more than 5-folds lower than that of 11-DCL. Therefore, these results confirm the ML MBene-aptasensor specificity and the absence of cross-reactivity towards other hormones and 11-DCL precursors. Our strategy thus presents a good alternative for immunoassays employed in CAH screening, where false positive results are very common because of the cross-reactivity of the 11-DCL antibody for other hormones.

In our previous report, we attributed the specificity of the 11-DCL aptamer to the absence of the hydroxyl group in contrast to its hydroxylated analogues, *i.e.*, cortisol, corticosterone, progesterone and pregnenolone, where the OH group creates a hydrophilic media that inhibit the aptamer binding.[28,38]

Finally, after the aptasensor validation in experimental conditions, we measured 11-DCL in real serum samples. First, serum samples were diluted (1 to 100) and spiked with two concentrations of 11-DCL (0.01 and 0.05 pg mL^{-1}). Afterwards, the two samples were incubated separately with the developed aptasensor. The analytical response ($(i^0 - i)/i^0$%) was then determined and compared to that obtained in the calibration curve. Very good recovery percentages (92.03% and 87.57%) were achieved, with good RSDs of less than 5%, for the triplicate trials. These results confirm the applicability of the ML MBene-based aptasensor for 11-DLC determination in serum samples.

Reproducibility, repeatability and stability

The reproducibility of the aptasensor was assessed to confirm that the fabrication conditions would not affect the accuracy of the proposed method. Three aptasensors were fabricated and tested with a fixed concentration (10 pg mL^{-1}) of 11-DCL. Under the optimized conditions, the analytical response was calculated for each sensor. The results showed relative standard deviations (RSDs) of less than 5%. In parallel, the stability was tested after 1, 3, 7, 30 and 90 days by storing the functionalized electrodes at 4 °C in a water-saturated atmosphere. No significant change was noted for the biosensor response towards 10 pg mL^{-1} of 11-DCL on the same day. Then, a maximum loss of activity of 12% was observed after 90 days with the MBene-based aptasensor.

Conclusion

Herein, a dual platform was constructed to compare the electrochemical properties of ML MBene and its parental precursor MoAlB MAB phase, and investigate their application in the aptasensing of 11-deoxycortisol. First, the MAB phase and ML MBene-modified electrodes were characterized electrochemically by cyclic voltammetry. The results obtained show that ML MBene exhibited better conductivity owing to its terminal groups and well-pronounced multilayered structure. Then, after adding the ssDNA aptamer on the two electrodes, we concluded that ML MBene offers excellent immobilization support for the aptamer. The ML MBene-based aptasensor was then applied for the detection of 11-DLC hormone. The proposed strategy has shown excellent analytical performance with the low detection limit of 0.014 pg mL^{-1}. Moreover, the aptasensor exhibited a high selectivity towards 11-DLC with negligible reactivity to 17-OH pregnenolone, 17-OH progesterone and 11-deoxycortisol molecules. Based on this study, we confirm that MBene holds great promise for application in electrochemical biosensing.

Author contributions

AR analyzed the electrochemical results, performed the structural analysis of the modified electrodes, designed the figures and wrote the original draft. RRM fabricated the aptasensors, and performed electrochemical characterization and detection experiments. MC prepared and characterized the MBene samples, collected and analyzed the obtained results, designed figures, and corrected the original manuscript draft. KE prepared the MAB samples. MN coordinated the synthesis of the MAB phase (MoAlB) and corrected the original manuscript. AJ acquired funds, coordinated the research, and corrected the original manuscript. MZ acquired funds, coordinated the research, and corrected the original manuscript. The manuscript was written with contributions from all authors. All authors have approved the final version of the manuscript.

Data availability

The data that support the findings of this study are available from the corresponding author upon reasonable request.

Conflicts of interest

The authors declare no conflicts of interest.

Acknowledgements

OPUS-18, UMO-2019/35/B/ST5/02538, National Science Center; Warsaw University of Technology within the Excellence Initiative: Research University (IDUB) programme, grant "MXenzymes as a new generation of nanozymes based on two-dimensional MXene materials". The authors would like to acknowledge the generous funding from the research and graduate office at Alfaisal University under grant number 1149. This work was funded by the National Science Centre (NCN) within the framework of the research project 'OPUS-18' (UMO-2019/35/B/ST5/02538).

References

1 L. Fu and W. Xia, MAX phases as nanolaminate materials: chemical composition, microstructure, synthesis, properties, and applications, *Adv. Eng. Mater.*, 2021, **23**(4), 2001191.
2 V. G. Nair, M. Birowska, D. Bury, M. Jakubczak, A. Rosenkranz and A. M. Jastrzębska, 2D MBenes: a novel member in the flatland, *Adv. Mater.*, 2022, **34**(23), 2108840.
3 N. F. Rosli, M. Z. M. Nasir, N. Antonatos, Z. k Sofer, A. Dash, J. Gonzalez-Julian, A. C. Fisher, R. D. Webster and M. Pumera, MAX and MAB Phases: Two-dimensional layered carbide and boride nanomaterials for electrochemical applications, *ACS Appl. Nano Mater.*, 2019, **2**(9), 6010–6021.
4 M. W. Barsoum, The MN+ 1AXN phases: A new class of solids: Thermodynamically stable nanolaminates, *Prog. Solid State Chem.*, 2000, **28**(1–4), 201–281.
5 M. Jakubczak, A. Wojciechowska, D. F. Zambrano, D. Moncada, M. Birowska, D. Moszczyńska, K. Eisawi, M. Naguib, A. Rosenkranz and A. M. Jastrzębska, Synthesis, properties and solid lubrication performance of MoAlB-based MBene, *Appl. Mater. Today*, 2023, **35**, 101925.
6 M. Naguib, V. N. Mochalin, M. W. Barsoum and Y. Gogotsi, 25th anniversary article: MXenes: a new family of two-dimensional materials, *Adv. Mater.*, 2014, **26**(7), 992–1005.
7 M. Jakubczak, A. Szuplewska, A. Rozmysłowska-Wojciechowska, A. Rosenkranz and A. M. Jastrzębska, Novel 2D MBenes—synthesis, structure, and biotechnological potential, *Adv. Funct. Mater.*, 2021, **31**(38), 2103048.
8 M. Ade and H. Hillebrecht, Ternary borides Cr_2AlB_2, Cr_3AlB_4, and Cr_4AlB_6: The first members of the series (CrB_2) n CrAl with n = 1, 2, 3 and a unifying concept for ternary borides as MAB-phases, *Inorg. Chem.*, 2015, **54**(13), 6122–6135.
9 D. Chen, Z. Jin, B. Zhao, Y. Wang and Q. He, MBene as a theranostic nanoplatform for photocontrolled intratumoral retention and drug release, *Adv. Mater.*, 2021, **33**(16), 2008089.
10 Y. R. Freund, T. Akama, M. Alley, J. Antunes, C. Dong, K. Jarnagin, R. Kimura, J. A. Nieman, K. R. Maples and J. J. Plattner, Boron-based phosphodiesterase inhibitors show novel binding of boron to PDE4 bimetal center, *FEBS Lett.*, 2012, **586**(19), 3410–3414.
11 S. Feng, Y. Yao, J.-C. Charlier, G.-M. Rignanese and J. Wang, h-MBenes (M/B = 1:1) as promising electrocatalysts for nitrogen reduction reaction: a theoretical study, *Chem. Mater.*, 2023, **35**(21), 9019–9028.
12 S. Wei, G. Kale and X. Lai, Unlocking Enhanced Electrochemical Performance of MBene-MoB Through Controlled Aluminum Dissipation from MoAlB, *Small*, 2024, 2401573.
13 C. Peng, X. Jiang, M. Jaeger, P. van Houten, A. E. van Herwaarden, V. A. Koeken, S. J. Moorlag, V. P. Mourits, H. Lemmers and H. Dijkstra, 11-deoxycortisol positively correlates with T cell immune traits in physiological conditions, *EBioMedicine*, 2024, **99**, 104935.
14 S. Chakraborty, J. Pramanik and B. Mahata, Revisiting steroidogenesis and its role in immune regulation with the advanced tools and technologies, *Genes Immun.*, 2021, **22**(3), 125–140.
15 M. K. Auer, A. Nordenström, S. Lajic and N. Reisch, Congenital adrenal hyperplasia, *Lancet*, 2023, **401**(10372), 227–244.
16 N. Janzen, F. G. Riepe, M. Peter, S. Sander, U. Steuerwald, E. Korsch, F. Krull, H. L. Müller, S. Heger and C. Brack, Neonatal screening: identification of children with 11β-hydroxylase deficiency by second-tier testing, *Horm. Res. Paediatr.*, 2012, **77**(3), 195–199.
17 F. Fanelli and G. Di Dalmazi, Serum steroid profiling by mass spectrometry in adrenocortical tumors: diagnostic implications, *Curr. Opin. Endocrinol., Diabetes Obes.*, 2019, **26**(3), 160–165.
18 F. Fanelli, S. Bruce, M. Cantù, A. Temchenko, M. Mezzullo, J. M. Lindner, M. Peitzsch, P.-A. Binz, M. T. Ackermans and A. C. Heijboer, Report from the HarmoSter study: inter-laboratory comparison of LC-MS/MS measurements of corticosterone, 11-deoxycortisol and cortisone, *Clin. Chem. Lab. Med.*, 2023, **61**(1), 67–77.
19 B. C. McWhinney, S. E. Briscoe, J. P. Ungerer and C. J. Pretorius, Measurement of cortisol, cortisone, prednisolone, dexamethasone and 11-deoxycortisol with ultra high performance liquid chromatography–tandem mass spectrometry: application for plasma, plasma ultrafiltrate, urine and saliva in a routine laboratory, *J. Chromatogr. B: Anal. Technol. Biomed. Life Sci.*, 2010, **878**(28), 2863–2869.
20 F. Fanelli, M. Cantù, A. Temchenko, M. Mezzullo, J. M. Lindner, M. Peitzsch, J. M. Hawley, S. Bruce, P.-A. Binz and M. T. Ackermans, Report from the HarmoSter study: impact of calibration on comparability of LC–MS/MS measurement of circulating cortisol, 17OH-progesterone and aldosterone, *Clin. Chem. Lab. Med.*, 2022, **60**(5), 726–739.
21 C. A. Shaughnessy, A. Barany and S. D. McCormick, 11-Deoxycortisol controls hydromineral balance in the most basal osmoregulating vertebrate, sea lamprey (Petromyzon marinus), *Sci. Rep.*, 2020, **10**(1), 12148.

22 C. A. Shaughnessy and S. D. McCormick, 11-Deoxycortisol is a stress responsive and gluconeogenic hormone in a jawless vertebrate, the sea lamprey (Petromyzon marinus), *J. Exp. Biol.*, 2021, **224**(11), jeb241943.

23 M. Bauer, M. Strom, D. S. Hammond and S. Shigdar, Anything you can do, I can do better: Can aptamers replace antibodies in clinical diagnostic applications?, *Molecules*, 2019, **24**(23), 4377.

24 L. Agnello, S. Camorani, M. Fedele and L. Cerchia, Aptamers and antibodies: rivals or allies in cancer targeted therapy?, *Explor. Targeted Anti-Tumor Ther.*, 2021, **2**(1), 107.

25 G. Contreras Jiménez, S. Eissa, A. Ng, H. Alhadrami, M. Zourob and M. Siaj, Aptamer-based label-free impedimetric biosensor for detection of progesterone, *Anal. Chem.*, 2015, **87**(2), 1075–1082.

26 J. A. Martin, J. L. Chávez, Y. Chushak, R. R. Chapleau, J. Hagen and N. Kelley-Loughnane, Tunable stringency aptamer selection and gold nanoparticle assay for detection of cortisol, *Anal. Bioanal. Chem.*, 2014, **406**, 4637–4647.

27 V. Skouridou, M. Jauset-Rubio, P. Ballester, A. S. Bashammakh, M. S. El-Shahawi, A. O. Alyoubi and C. K. O'Sullivan, Selection and characterization of DNA aptamers against the steroid testosterone, *Microchim. Acta*, 2017, **184**, 1631–1639.

28 S. Eissa, A. Siddiqua, R. Chinnappan and M. Zourob, Electrochemical SELEX technique for the selection of DNA aptamers against the small molecule 11-deoxycortisol, *ACS Appl. Bio Mater.*, 2019, **2**(6), 2624–2632.

29 M. Naguib; M. Kurtoglu; V. Presser; J. Lu; J. Niu; M. Heon; L. Hultman; Y. Gogotsi and M. W. Barsoum, Two-dimensional nanocrystals produced by exfoliation of Ti_3AlC_2, *MXenes*, Jenny Stanford Publishing, 2011, pp. 15–29.

30 K. R. G. Lim, M. Shekhirev, B. C. Wyatt, B. Anasori, Y. Gogotsi and Z. W. Seh, Fundamentals of MXene synthesis, *Nat. Synth.*, 2022, **1**(8), 601–614.

31 L. T. Alameda, C. F. Holder, J. L. Fenton and R. E. Schaak, Partial etching of Al from MoAlB single crystals to expose catalytically active basal planes for the hydrogen evolution reaction, *Chem. Mater.*, 2017, **29**(21), 8953–8957.

32 A. Majed, M. Torkamanzadeh, C. F. Nwaokorie, K. Eisawi, C. Dun, A. Buck, J. J. Urban, M. M. Montemore, V. Presser and M. Naguib, Toward MBenes Battery Electrode Materials: Layered Molybdenum Borides for Li-Ion Batteries, *Small methods*, 2023, **7**(8), 2300193.

33 S. S. Sangu, N. M. Illias, C. C. Ong, S. C. B. Gopinath and M. S. M. Saheed, MXene-based aptasensor: characterization and high-performance voltammetry detection of deoxynivalenol, *Bionanoscience*, 2021, **11**, 314–323.

34 D. Bury, M. Jakubczak, M. A. K. Purbayanto, M. Rybak, M. Birowska, A. Wójcik, D. Moszczyńska, K. Eisawi, K. Prenger and V. Presser, Wet-Chemical Etching and Delamination of MoAlB into MBene and Its Outstanding Photocatalytic Performance, *Adv. Funct. Mater.*, 2023, **33**(50), 2308156.

35 Y. Li, H. J. Schluesener and S. Xu, Gold nanoparticle-based biosensors, *Gold Bull.*, 2010, **43**, 29–41.

36 H. Meskher, T. Ragdi, A. K. Thakur, S. Ha, I. Khelfaoui, R. Sathyamurthy, S. W. Sharshir, A. Pandey, R. Saidur and P. Singh, A review on CNTs-based electrochemical sensors and biosensors: unique properties and potential applications, *Crit. Rev. Anal. Chem.*, 2023, 1–24.

37 A. Szuplewska, D. Kulpińska, M. Jakubczak, A. Dybko, M. Chudy, A. Olszyna, Z. Brzózka and A. M. Jastrzębska, The 10th anniversary of MXenes: Challenges and prospects for their surface modification toward future biotechnological applications, *Adv. Drug Delivery Rev.*, 2022, **182**, 114099.

38 K.-A. Yang, H. Chun, Y. Zhang, S. Pecic, N. Nakatsuka, A. M. Andrews, T. S. Worgall and M. N. Stojanovic, High-affinity nucleic-acid-based receptors for steroids, *ACS Chem. Biol.*, 2017, **12**(12), 3103–3112.